INTERNATIONAL ATOMIC ENERGY AGENCY
UNITED NATIONS EDUCATIONAL, SCIENTIFIC AND CULTURAL ORGANIZATION
INTERNATIONAL CENTRE FOR THEORETICAL PHYSICS
I.C.T.P., P.O. BOX 586, 34100 TRIESTE, ITALY, CABLE: CENTRATOM TRIESTE

H4.SMR/383 - 22

WORKSHOP ON REMOTE SENSING TECHNIQUES WITH APPLICATIONS TO AGRICULTURE, WATER AND WEATHER RESOURCES

(27 February - 21 March 1989)

TOPICS IN CLOUD PHYSICS RELEVANT TO RADAR METEOROLOGY

FRANCO PRODI
FISBAT Institute - CNR
Via de' Castagnoli, 1
40126 Bologna
ITALY

TOPICS IN CLOUD PHYSICS
RELEVANT TO RADAR METEOROLOGY

F. Prodi

FISBAT, National Research Council - Bologna

Introduction

The radar has been used in meteorology when cloud physics was still in its infancy and its main achievements were still to come; so it is hard to establish which one of the two research fields, cloud physics and radar meteorology, took more benefit from the other. All along the last 30 years it is quite easy to find examples of beneficial interactions. Cloud physics was helping radar meteorology enlightning the properties and behaviour of cloud particle populations, the processes, and time sequence, of precipitation formation, the hydrodynamic behaviour of hydrometeors, having in turn from the radar, to mention a remarkable example, the observation of the bright band in stratiform clouds, which not only confirmed the Bergeron-Findeisen process but indicated features of aggregation and melting of snowflakes. Radar meteorology could also gain unexpected insights into such an arcane topic as storm dynamic showing new radar features as the echo free vault, the wall and so on which stimulated new ideas in storm dynamics.

Now more than ever, though the communities of cloud physicists and radar meteorologists operate almost completely (and I would say, unfortunately) separated, areas of positive interaction are expanding. The development of new concepts in radars (multiple wavelengths, Doppler, polarization diversity) or the new wavelengths explored (notably by the millimetric radars) are posing many interesting questions, as well as stimulus, to the cloud physics community. The evolution of cloud physics itself from microphysics oriented to dynamic or mesoscale oriented has certainly to do with the stimuli impressed by radar meteorology.

The purpose of this lecture is to survey the areas of interaction between the two fields, mostly in the direction cloud physics (c.p.) to radar meteorology (r.m.). From what we have mentioned before the reverse title (topics in r.m. relevant to cloud physics) would have been equally possible, but it is obvious that we must circumscribe our subject. We must foretell also that for the different topics, we will not investigate the full applicability in radar meteorology, but we will simply indicate which branch of it is likely to be more affected. Moreover, and quite obviously, this survey does not pretend to be exhaustive or even to touch the most important topics.

The general problem in radar meteorology is to have the backscattered signal produce the largest information on the properties of the target (mostly hydrometeors) in the backscattering volume. Since this is of the order of 10^6 m^3, even at the short ranges, a great variety of situations (in terms of type of hydrometeors, their concentration and size distributions, surface characteristics, etc.) is possible in it, producing a given signal. Any knowledge we can obtain, from the intrinsic development of cloud physics, on the behaviour of the hydrometeor populations representing the (fluctuating) radar target is useful for the interpretation of the backscattered signal.

We will investigate some of the mechanisms of hydrometeor growth and interaction relevant to this interpretation. They can be classified according to the main processes involved into:

- warm rain mechanisms: collision, coalescence and break-up
- cold rain mechanisms: droplet accretion on ice crystals, growth, melting and shedding of graupels and hailstones, hailstone characteristics.

The effects of electric fields in modifying drop shapes will also be investigated.

Finally, a remarkable and recent example of beneficial interaction between cloud physics and radar meteorology will be shown.

The importance of the mentioned mechanisms is different depending on dealing with radar signals near to the ground or aloft. Radar reflectivity near the ground has been related to precipitation intensity in innumerable studies, and is the subject of most lectures in this seminar. A number of relations between the rainfall rate R at the ground and radar reflectivity factor Z have been derived, using either measurements of rainfall with raingauges and observed values of Z, or measurements of the size distributions of the drops and computed values of Z.

Instead, radar reflectivity aloft is much more difficult to interprete due to the complex phenomenology. Precipitation particles in strong updrafts are lifted high into the zone of supercooling during the early stages of their growth, and become at least partially frozen or develop into hail. A considerable fraction of the cloud water accreted by small hailstones is likely to remain unfrozen in wet or spongy hailstone fabrics, or are shed as drops of liquid water in the wake. Moreover, hailstone surfaces are expected to have dry surfaces only above the top of the zone of supercooling and to be wet elsewhere. In addition, though locally the precipitation particles can be uniform in size, they are generally present in wide ranges of sizes, have generally aspherical shapes and during fall have a variety of orientations. Ice crystals in turn can capture supercooled droplets or aggregate to form snowflakes.

The scattering of centimetric wavelength radiation by the hydrometeors aloft is strongly dependent upon their size, shape, orientation and composition, and quite often only general interferences about the identity and concentration of precipitation can be made from measurements of radar reflectivity by conventional radars.

1. WARM RAIN

Collision-coalescence

We look at the collission-coalescence process which is still unknown, except for:

a - the collision efficiency is not 1;

b - calescence may result from one out of 4-8 even 10 collisions.

Instead, cloud models in general assume that droplets in the swept out volume of a larger one will collide and consequently coalesce.

In a recent paper (Low and List, 1982) an attempt is made to fit the experimental data on coalescence. When coalescence occurs there is a net loss of surface area, because the newly-formed drop has a smaller surface in the spherical approximation, than the total surface area of the original colliding drops. This decrease can be expressed as:

$$\Delta S_\sigma = S_T - S_c$$

where the total surface energy of the incident drops is:

$$S_T = \pi\sigma \left(D_L^2 + D_S^2 \right)$$

is the surface tension of water ($7.28\ 10^{-2}$ N m^{-1} at 20°C) and:

$$S_c = \pi\sigma \left(D_L^3 + D_S^3 \right)^{2/3}$$

S_c is the surface energy of the spherical equivalent of the united drop mass.

ΔS_σ becomes increasingly important as the colliding drops become smaller.

For coalescence to occur, both collision kinetic energy (CKE) and ΔS_σ must be adequately dissipated by the coalesced drop. This is accomplished by the oscillations and deformations of the liquid drop. The deformed drop passes the energy off to the air by way of drag and dissipates it internally through the viscous action of the water itself. However, any model of the collision process based on the oscillation of the spheroidal drop would be quite complex, as the fundamental modes of oscillation prove inadequate and higher order oscillations must be included.

In Fig. 1 (Low and List 1982) the values of the coalescence efficiency are given, calculated for raindrop pairs with diameters D and D_s; no coalescence occurs in the hatched area.

As for the brenk-up, experimentally measured spectra are available. Fig. 2 gives fragment distributions for 4 mm diameter drops colliding with 0.5 mm to 3.5 mm small drops. The curves as the sizes of the small droplets change, represent a 3D surface.

The results were used by Gillespie and List (1979) in modelling a steady state infinitely wide rainshaft where the raindrop source at the 2 km level produced particles with a Marshall Palmer distribution.

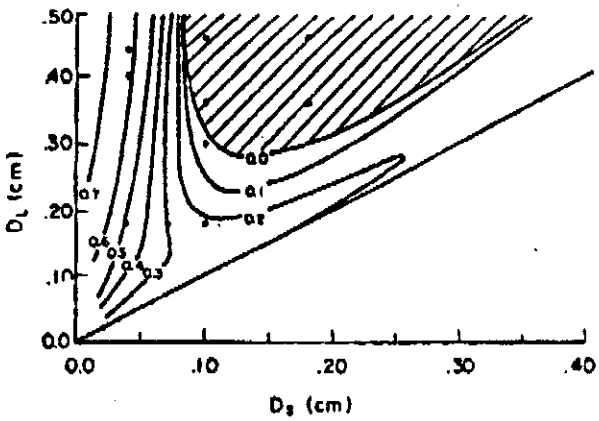

FIG. 1 Values of the parameterized coalescence efficiency E_{coal} of all drop pairs of sizes D_L and D_S. The studied drop pairs are indicated by dots. The straight line $D_L = D_S$ corresponds to a value of $E_{coal} = 0.19$.

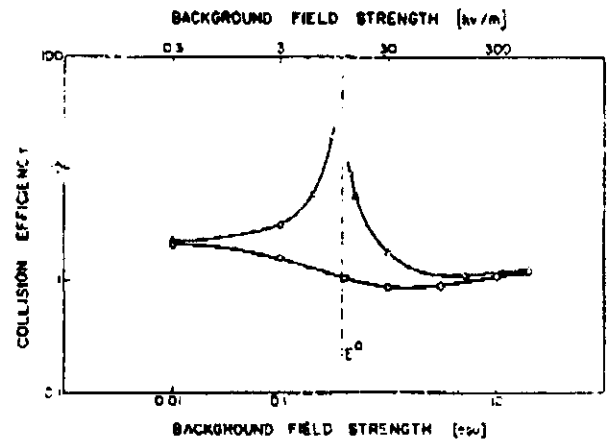

Fig. 2 – *Collision efficiencies of the (10.9) μm radius droplet pair as function of the background field (parallel to gravity). Triangles represent configuration 4 (Q_1 negative $= -Q_2$), circles configuration 3 (Q_1 positive $= -Q_2$). The critical field for equal fall velocity for $Q_1 \sim 3.34 \times 10^{-14}$C $= 10^{-4}$ esu is $E^* = 11.07$ kVm^{-1}. The viscous collision efficiency is 0.013* (FREIRE & LIST, *1979*).

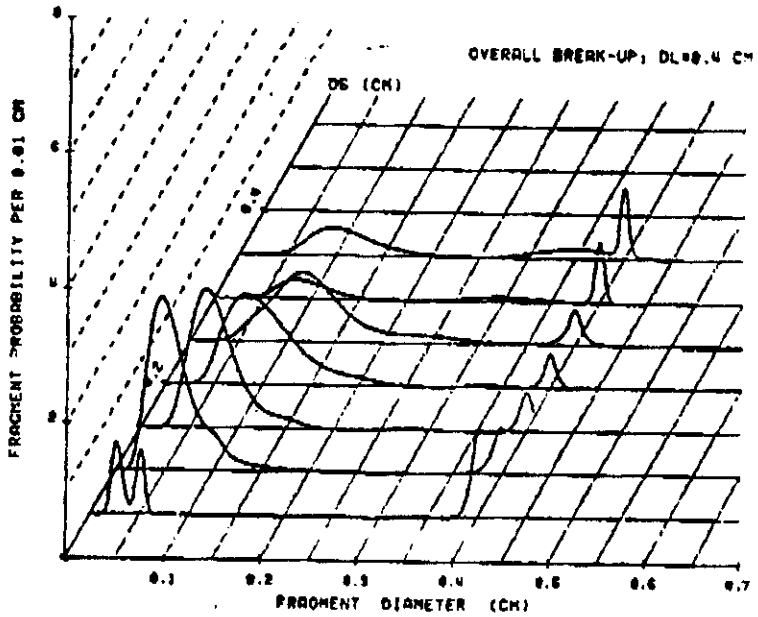

FIG. 3 Average fragment number distributions for overall breakup, for different small drop diameters D_S, for a large drop diameter $D_L = 0.40$ cm. Note the small ridge of fragments echoing the original small drop approaching the large fragments (remnants of the large drops D_L) for $D_S \rightarrow D_L$, and the independent ridge of the smaller fragments.

Air is a third body in the collision break-up and has an effect on the fragment distribution.

The story of collision is further complicated by electrical effects. Since collision coalescence is particularly slow, in a cloud where only small droplets are found with respective collision efficiency much smaller than 1, electrical effects enhance greatly collision probability and the cloud evolution is accelerated. Freire and List (1979) carried out collision efficiencies calculations for specific configurations, with collision efficiencies orders of magnitude larger than the pure viscous flow ones (Fig. 3).

2. COLD RAIN

The rain in middle latitudes originates in cloud regions with temperatures below freezing from ice particles which freeze at the expense of the surrounding supercooled droplets. Ice crystals grow from nuclei first by water vapour diffusion, then by accretion of cloud droplet and by aggregation of other ice crystals. The crystals accreting droplets or a large frozen droplet can become an embryo of graupel, small hail and hailstones. The process of melting of these hydrometeors and shedding or melting of hailstones themselves lead to the production of large droplets. Practically all these processes have relevance to radar meteorology.

We will consider in some detail the growth of crystals by inertia capture of droplets, the melting of hailstones and graupels, and the deformation of the drop shape of increasing size and due to external electric fields.

Inertia capture of droplets by ice crystals

The quantitative treatment of the stage of growth of ice crystals is limited by the incomplete knowledge of the collection efficiencies of the different crystal shapes for the various sizes of water droplets.

The cut-off diameter of droplets accreted on real columnar and dendritic crystals (ONO, 1969) and plate-like and dendritic (Harimaya, 1975) have been observed to be between 10 and 20 μm. For particles of this size the only important capture process is the inertial or aerodynamic capture, as phoretic forces are not effective and electrostatic effects are considered to be negligible. In the conditions in which the aerodynamic capture is effective the characteristics of the fluid motion have a wide range of variability due to the different flow velocities (in this case the terminal velocities of droplets and crystals). The flow characteristics are determined by a set of numbers which indicate the relative importance of the acting forces: the Reynolds number, the Stokes number, and the Froude number. The Reynolds number describes the balance between inertial and viscous forces of the fluid near the obstacle. At low N_{Re} the viscous effect is dominant and the flow is described by the Navier Stokes equation in which the viscous dissipation terms are maintained. In the range 100-3000 the fluid motion is still laminar but the viscous terms can be neglected, and the fluid is well

described by the Euler equation: as the velocity field is expressed in terms of a gradient of a scalar function the corresponding flow regime is named potential flow. The range $1 < N_{Re} < 100$ defines a region of transition from the viscous flow to potential flow and is typically the range of the inertial capture of droplets by ice crystals in clouds. In this transition region the solutions for viscous flow or potential flow are derived as approximation of the actual flow. The main problem in this region is to determine the fluid-obstacle interaction, through the drag coefficient C_d which is not given by the theory. Similarity experiments allow the drag coefficent to be determined as a function N_{Re}. However in complex systems such as the particle-obstacle interaction, similarity conditions cannot be satisfied simultaneously for all the numbers characterizing the fluid motion and the particle-obstacle interaction. This is the reason for simulation experiments to be performed, in which the capture process is reproduced in the laboratory for particles and obstacles of various shapes to derive experimental collection efficiencies, to be compared with the values given by potential or viscous flow theories.

We have performed such experiments (Prodi et al., 1981) in a wide range of Stokes numbers with planar and stellar models as obstacles in the intermediate range of flow, taking advantage also of the recent improvements in the generation of monodisperse spherical particles.

The experiments have been performed in a downward continuous vertical flow with the obstacle fixed in the rear, on the tip of a long vertical needle along the axis of the cylindrical pipe. In Fig. 4 the planar shapes tested in the experiments are shown and details with the captured particles. The characteristics of the particles used in the test are given in the table. The results of the collection efficiency of disks versus Stokes numbers are given in the Fig. 5. Other experimental results and theoretical curves from potential and viscous flow are also drawn for comparison. The results show that the data are much better fitted, in the 0.7 to 4 N_{St} numbers by the viscous flow curves and support the validity of the approach used in the Pitter and Pruppacher model.

At $N_{St} < 0.7$ the theoretical curves show a cutoff, while our experimental results present low non zero collision efficiencies down to N_{St} around 0.2. In the range $N_{St} > 4$ our experimental conditions depart from those described by the theoretical curves of Pitter and Pruppacher model, which refer to velocities of droplets relative to the falling oblate spheroid. While the Stokes number accounts for the relative velocity the Reynolds number is based on the fall. velocity of the obstacle. So curves for different Reynolds numbers depart, when drawn as a function of the Stokes number and the comparison of our experimental data with the theoretical curves is no longer possible.

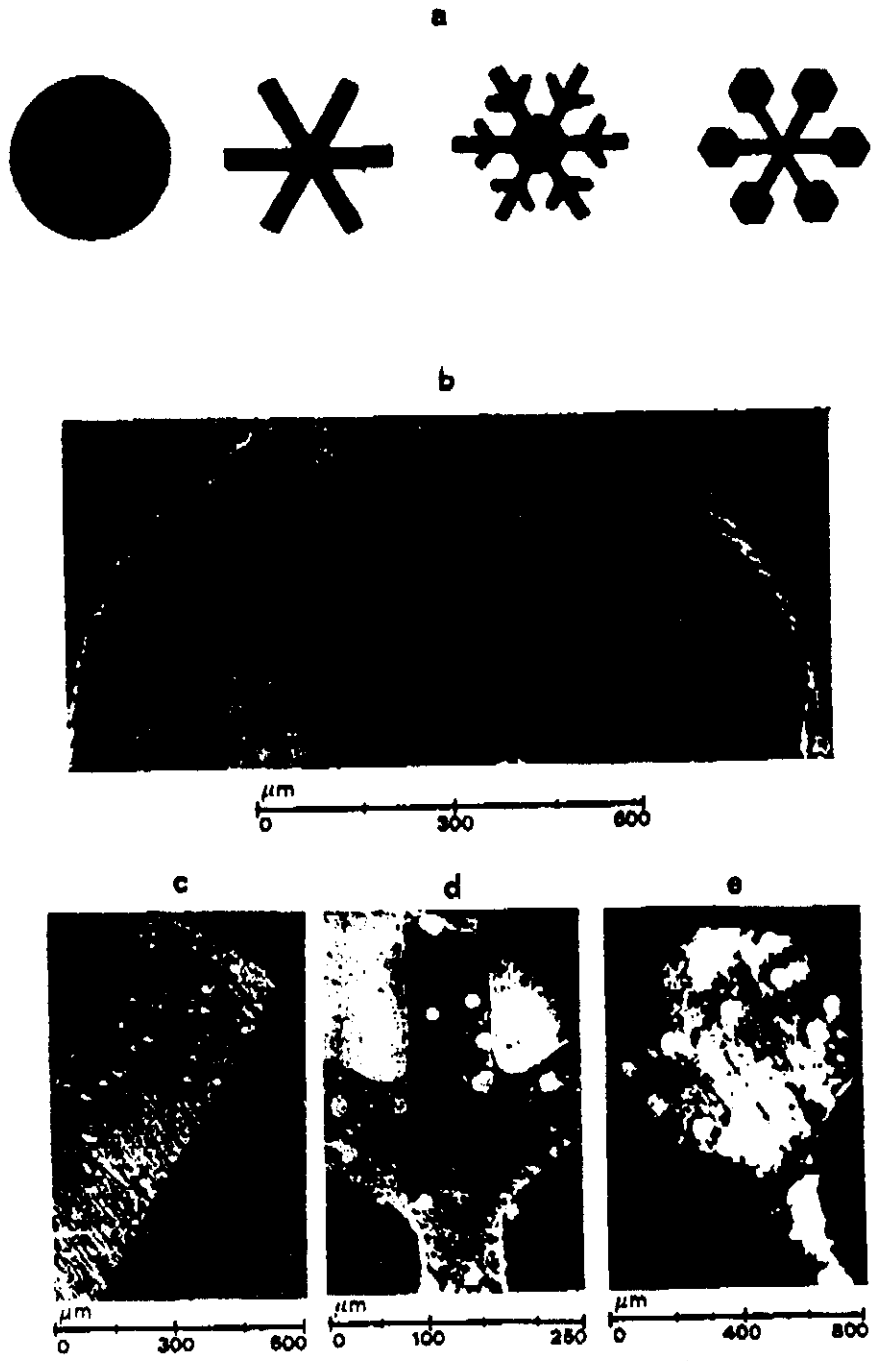

Figure 4 (a) Different planar shapes tested in the experiments. From right to left: disk, stellar, ordinary dendritic and stellar with plates at ends.
(b) Detail of the disk shaped obstacle (1200 μm size) with captured Lycopodium spores.
(c) Detail of a tip of the stellar shaped obstacle with captured oil droplets.
(d) Detail of the ordinary dendritic shaped obstacle, with captured Lycopodium spores.
(e) Detail of the planar shaped obstacle with hexagons at ends with captured Hicory Pecan poliens.

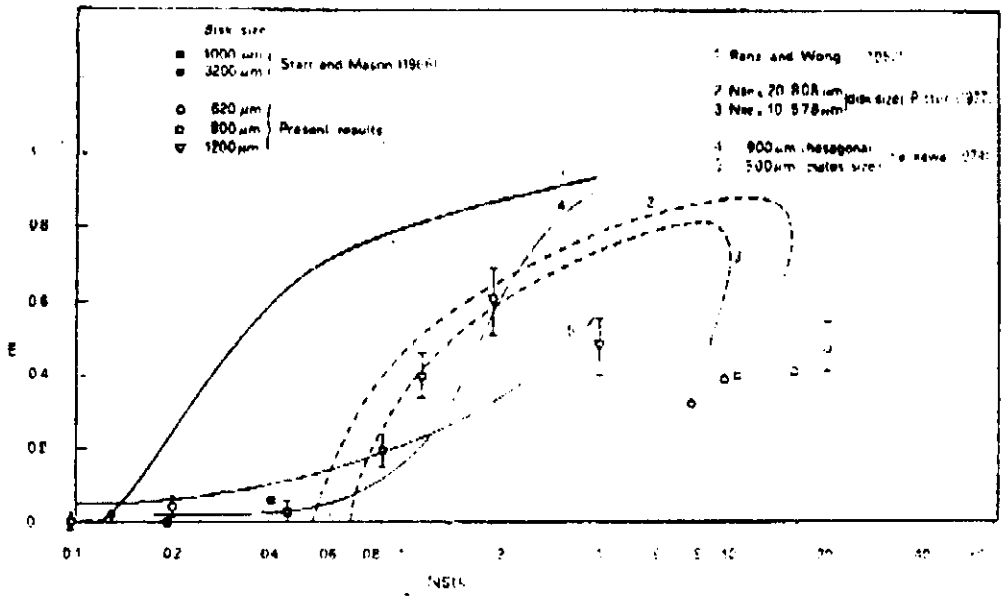

Figure 5 Collection efficiency of disks vs. Stokes number. Open symbols refer to the present experiments. The error bars are reported for sets of more than three experimental runs. Other experimental results and theoretical curves from potential and viscous flow are also drawn for comparison.

3. GROWTH AND MELTING OF GROUPELS AND HAILSTONES

(a) Growth of hailstones and hailstone characteristics

Water molecules dipoles can be lined up by electric fields, leading to a polarization of the drop or of the liquid layer as a whole. Instead water molecules in the crystal lattice occupy almost fixed positions in a way to induce a lower refractive index with respect to water. So, as it is well known, the radar backscattering cross section is different in the two cases.

The treatment of radar backscatter by spherical and non spherical hailstones, dry or covered by a liquid layer, all solid or grown spongy, is a classical topic in radar meteorology and can be found in textbooks as the Battan book, besides being the subject of a specific seminar in this school. Summarizing the results, the radar reflectivity factor Z_e associated with solid spherical hailstones in a mass concentration of 1 $g.m^{-3}$ depends upon their size and the radar wavelength in the manner shown in Fig. 6. Theoretical calculations indicate that if the spheres have a sufficiently thick outer coat of liquid, they can behave as liquid spheres of the same size and can be said to be electromagnetically wet with radar reflectivity factors also shown in the figure. The thickness of the coast during melting of an ice sphere is of the order of 10^{-2}cm, and the effect of a film of such thickness on the backscattering cross section of a hailstone depends broadly on its size and the wavelength.

Also, the presence of internal liquid, acquired during growth in the wet regime, may substantially affect the backscatter from hailstones; such effects have been investigated in the laboratory. It was found that the radar cross section was almost unaffected by the composition of a core of diameter up to half the total diameter (and containing onle one-eighth of the total mass). Since the sequence of the layers is likely not affecting the backscattering cross section, the value of the spongyness ratio (liquid water to total mass ration) appears to be the most important property of the hailstone.

Therefore, to determine by hailstone analysis, the hailstone conditions during growth in the cloud (at the moment of radar observation) is of great importance also for interpreting the backscattered signal.

This knowledge in interpretation of the internal features of hailstones is rapidly progressing (also through a series of investigations in our laboratory, Levi and Prodi, 1978, Prodi and Levi, 1980) in a way that the growth conditions aloft can be assessed for each layer with an error of less than 3°C for the air and deposit temperatures (Fig. 7).

We do not enter deeply now into this interesting field of hailstones interpretation which also promises to be of help to radar meteorologists, but rather we focus on new results obtained by Prof. Pruppacher and his co-workers on the observation of the process of melting of ice hydrometeors, mostly groupels.

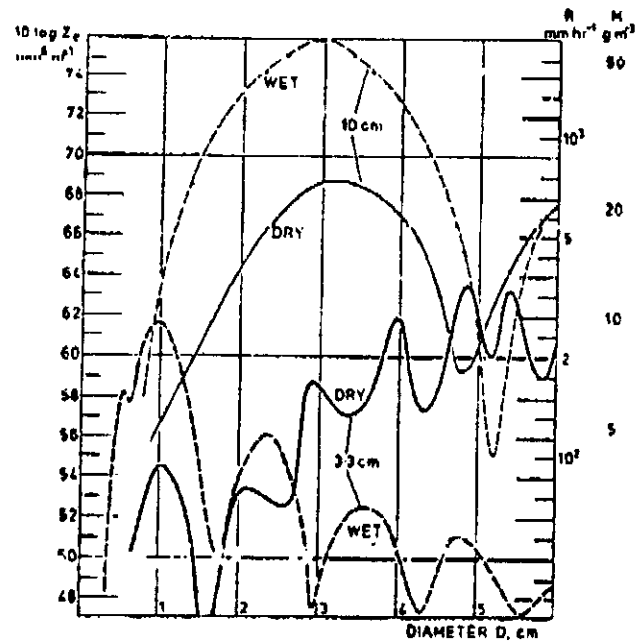

Fig. 6 The variation at two radar wavelengths of the reflectivity factor Z_e (mm^6 m^{-3}), expressed as $10 \log Z_e$, with the uniform diameter D (cm) of a mass concentration of 1 g m^{-3} of spherical hailstones, according to whether they are electromagnetically "dry" (behaving as pure ice) or "wet" (behaving as liquid water spheres of the same size; 187). The scales at the right show the mass concentration of rain M (g m^{-3}) and the rainfall rate at the ground R (mm hr^{-1}) corresponding to the same radar reflectivity ($Z = Z_e$), according to the relations (8.6) and (8.7).

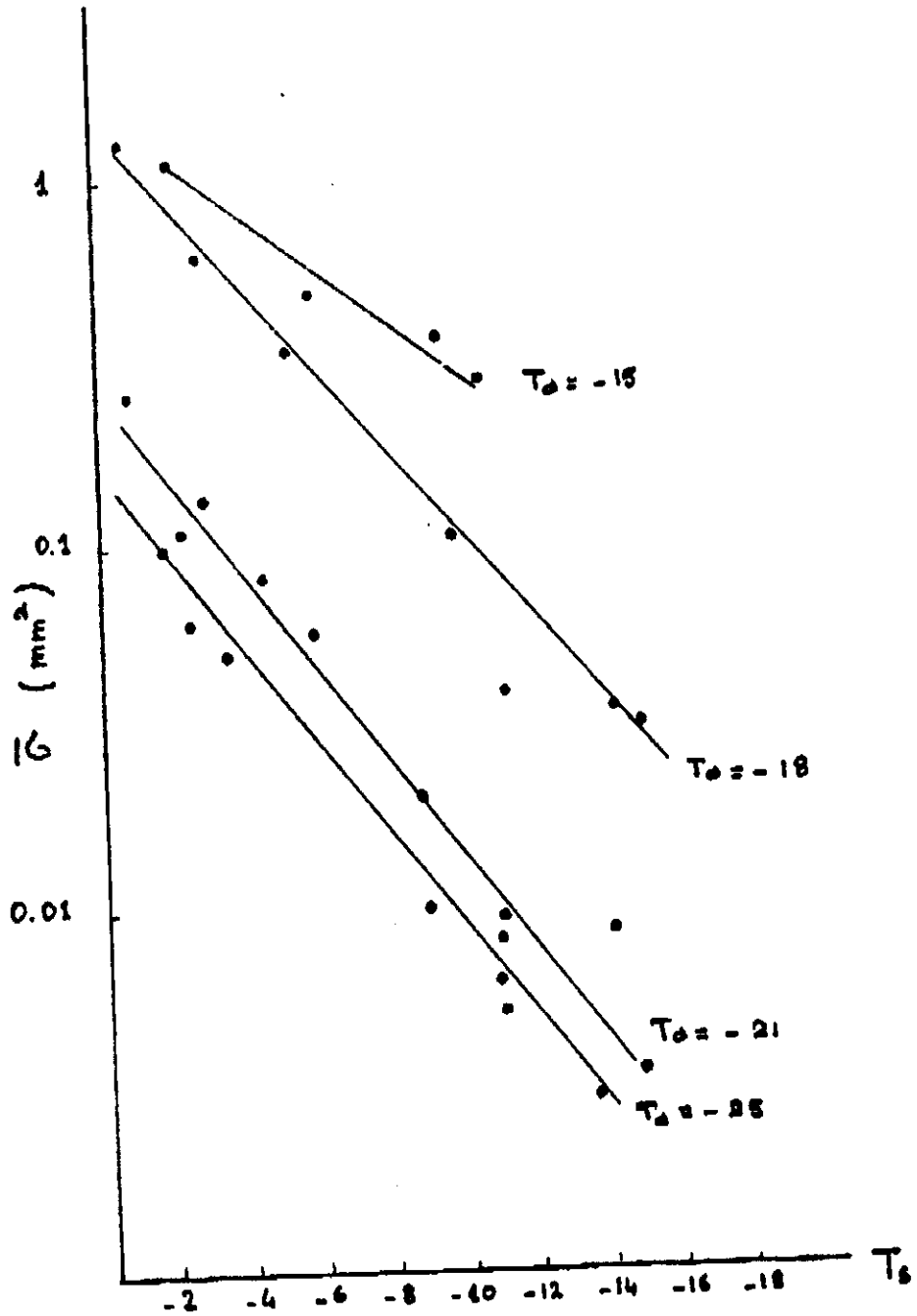

Fig. 7 Average grain size , as a function of the deposit temperature T_s, for artificial accretions of ice grown at various air temperatures T_a.

(b) Melting of groupels and small hail

A recent study (Rasmussen, Levizzani and Pruppacher, 1982) has shown the modes of a large ice sphere simulating the melting modes of natural hailstones. Wind tunnel experiments have shown that the melting process develops through the same steps, in the different experiments, from the initial to the final situation. A sphere 20 mm in diameter has been initially taken, suspended in the airflow by a thread. When it starts melting, a torus of liquid water forms at the equator of the ice particle and small water droplets are continuously shed. As the melting progresses the torus increases and shedding becomes intermittent (Fig. 8). This process continues until the meltwater forms a stable (huge) raindrop shape around the ice core: at this stage the diameter of the ice core is between 5 and 9 mm and no shedding occurs. When the diameter is between 1 and 5 mm the system is something similar to a raindrop on a conical core.

An even more interesting result, from the tunnel experiments, is that the ice core is remarkably eccentric with respect to the external melt sphere. As shown in Fig. 9 for an ice sphere at the last stage of melting (diameter of about 5 mm to a few hundred microns) the ice core is very close to the top of the water drop, and this position is maintained until the melting is completed. This feature is expected to have consequences on the radar backscattered signal for the reasons we have mentioned before.

The melting process we have described takes a defined period of time to be completed because of the finite rate of heat transfer to the melting ice core. For the computation it is considered a spherical ice particle of relatively large radius a, falling at terminal velocity in air of constant humidity and constant temperature $T_\infty > T_o = 273{,}15°C$. Since $T_\infty > T_o$ the ice particle melts and, assuming a spherical symmetry, at the time t is surrounded by a uniform water layer of thickness (a-r), where r = r(t); neglecting the shedding of water droplets and the evaporation, which means a = const, and assuming a steady state, the rate of release of latent heat of melting must be balanced by the rate of heat transfer through the water layer, so that equation may be written:

$$4\pi\rho_i L_m r^2 \frac{dr}{dt} = \frac{4\pi a r K_w [T_o - T_s(r)]}{(a-r)}$$

where: ρ_i = ice density
L_m = melting latent heat
K_w = thermal conductivity of water
T_o = temperature at the surface of the liquid layer
T_s = temperature at the ice-water interface
a = radius of water
r = radius of ice

Integrating we can calculate the melting time t_m

$$t_m = \frac{L_m \rho_i}{K_w} \int_r^a \frac{r(a-r)}{T_o - T_s(r)}\, dr$$

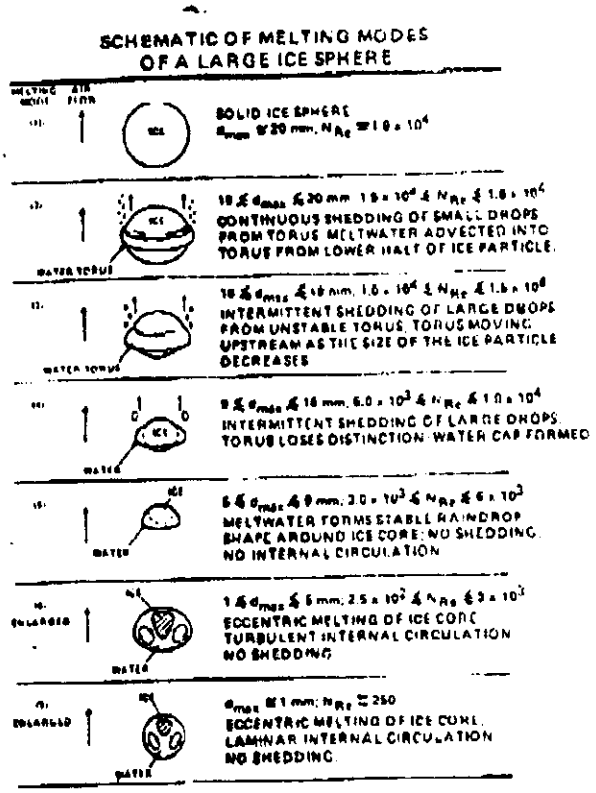

Fig. 8 Scheme of melting model of a large ice sphere

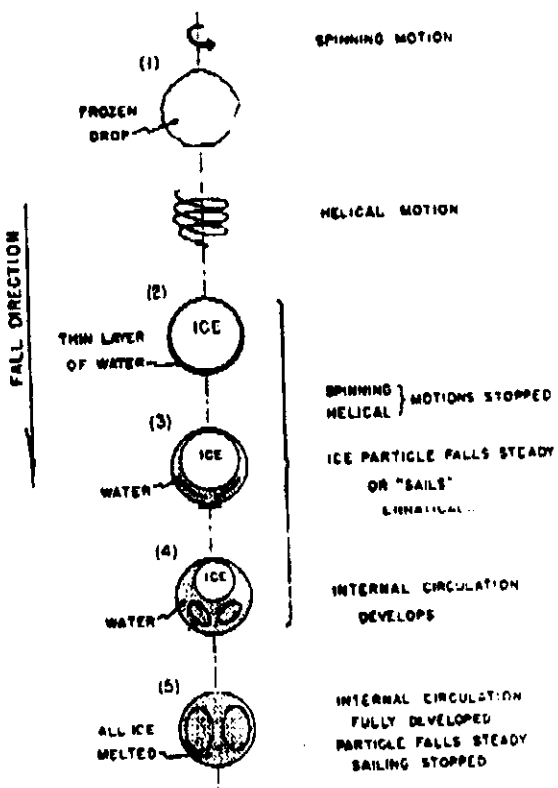

FIG. 9 Schematic of the actual melting behavior of a spherical ice particle, as revealed by motion pictures taken during present experiments

For steady state the rate of heat transfer through the water layer is balanced by the rate of heat dissipation by forced convection and evaporation at the surface of the ice particle. So Ta(r) is derived by

$$\frac{4\pi K_w a\, b\,[T_o - T_a(a)]}{d-a} = -4\pi a\, K_a\,[T_o - T_a(a)]\,\bar{f}_h - 4\pi a^2 L_e D_v (\rho_{vo} - \rho_{va})\,\bar{f}_v$$

where Ka is the thermal conductivity of air, $\bar{f}h$ and $\bar{f}v$ are ventilation coefficients for the thermal and diffusional terms respectively.

As shown in Fig. 8 and 9, especially at the final stages of melting, convection is present inside the water layer around the melting ice. When the diameter is below 5 mm the velocity of the fluid is very high and this clearly affects the melting behaviour of the ice particles. This kind of fast motion may also affect the backscattered signal; it seems that this effect has not been considered yet.

In summary, a better knowledge of the process of melting is needed in order to correctly interprete the radar return.

4. SHAPES OF UNCHARGED RAINDROPS IN EXTERNAL ELECTRIC FIELD

The shape of cloud particles appears to be an important parameter, as non-sphericity induces asymmetries in the backscattered radiation field. This effect enables us to discriminate between hail and rain, to determine raindrop size distributions and rainfall rates from radar observations. An experimental study of the deformations of the uncharged raindrops in an external electric field has been carried out recently using a cloud tunnel (Pruppacher et al., 1981) and the results appear of great interest. To simulate the situation of a vertical electric field, the droplets are freely suspended in the wind tunnel between the two plates of a condenser. The condenser was formed by two net screens and their distance was variable as their potential. In this way a variety of different cases was examined, varying the electric field and the drop size.

The results show that while the hydrodynamic forces tend to deform the drops into an oblate spheroid, electrical forces tend to impose a more spherical shape. The effects of the electric forces increase with increasing drop size so that the hydrodynamically caused deformation is counteracted with increasing efficiency. Therefore, for large drops the shapes can become spherical or even prolate spheroidal from the oblate spheroidal of an external field.

The break up behaviour can also be affected by the presence of an external electric field. In fact the break up of a large drop in the absence of an electric field is caused by the hydrodynamic forces acting on the lower side of the drop, i.e. upstream. Drop break up in the presence of an electric field proceeds via instabilities on the upper side, i.e. downstream. The authors suggest that for low external fields the hydrodynamic forces dominate and the electric forces have a small effect downstream on the drops where the flowfield is weak. At increasing electric fields the drop deforms rapidly; eventually, near the breakdown values the hydrodynamic forces lose their effect, in the drop's downstream side.

The steady state assumption has been made through this work; in reality, the drops strongly oscillate due to turbulence and other effects. Therefore, the same authors are performing measurements of oscillation frequencies and amplitudes.

5. EFFECTS OF HYDROMETEOR SHAPES ON POLARIZATION DIVERSITY RADARS

The effects of such a phenomenology are quite evident in polarization diversity radars, which are able to detect non spherical particles.

The depolarization ratio measured is the ratio of the power in the cross polarized plane P_c to that in the parallel polarized plane P_p, which is expressed in decibels as follows:

$$D_p(dB) = 10 \log \frac{P_c}{P_p}$$

Water droplets with axial ratios close to 0.1 lead to depolarization ratios of 10 to 30% for oblate and prolate spheroids respectively. For ice particles the value is about 3% at axis ratio 0.1 due to the low dielectric constant of ice. With randomly oriented spheroids the depolarization is less than 1 and D_p is negative, ranging from about -10 to -25 dB.

A different method of studying the shape of precipitation particles is that using circular polarization. When circularly polarized waves are scattered by spherical particles the backscattered signal is also circularly polarized, but at an opposite direction of rotation with respect to the incident signal. However, an antenna transmitting circularly polarized waves with one direction of rotation only accepts waves with the same direction of rotation. Therefore, a circularly polarized radar beam would not detect a shower of perfectly spherical particles. A system making use of circularly polarized waves for the study of particle shapes uses a single antenna which alternately radiates plane polarized waves and circularly polarized waves. The ratio of backscattered powers P_{circ}/P_{plane} is the cancellation ratio and can be expressed in decibels as

$$\text{cancellation (db)} = 10 \log P_{circ}/P_{plane}$$

For randomly oriented scatterers the cancellation ratio is less than unity and depolarization is 3 db greater than the cancellation.

Finally, the CDR radars or Circular Depolarization radars transmit left-handed circular polarized radiation (LHC) and receive both right-handed (RHC7, referred to as the main channel, and left-handed, the cross channel. These radars can produce particle vertical motion, CDR and the height and aspect of CDR. (Kropfli et al., Pasqualucci etc.).

CDR is defined as:

$$CDR = 10 \log P_L/P_R$$

P_L = power received in the left hand channel

P_R = power received in the right hand channel

If the scatterers are perfect spheres the "depolarization" is theoretically zero and no power is received.

Results by Pasqualucci etc. indicate that in mature and precipitation clouds the power received in the "cross polarized" or left hand channel is 10 to 20 dB below the received power in the main channel, i.e. $-20 \leq CDR \leq -10$. Increasing CDR for a given particle refractive index is associated with increasing particle deformity.

We look now at typical results obtained by Kropfil et al. With a series of high elevation scans through a moderate squall line they obtained profiles of vertical motion of the particles and CDR. Changes in CDR and the aspect dependency of CDR appeared to be associated with changes in the position in the fall speed diagram, confirming that CDR is responding to changes in particle type, and that perhaps the combination of fall speed and CDR data can provide more information about particle type than either can separately.

A more complex analysis of CDR data has been suggested by Moninger et al., 1982, during CCOPE observations using the scattering matrix. In Fig. 10 cross correlation data for a lightly precipitating stratiform cloud is given. Four regions are evidenced: sub-cloud, bright band, mid-cloud and cloud top. There is evidence of oriented Rayleigh scatterers in the sub-cloud and mid-cloud regions. In the bright band and cloud to regions oriented non-Rayleigh scatterers dominate the phase of the returned signal. This evidence of orientation in the bright band was a surprise, because the low values of ρ had suggested that tumbling generated by melting could dominate the return signal. However, if we remind ourselves of the work of Rasmussen et al. presented in this lecture showing that melting is stabilizing the hydrometeor, the orientation in the bright band can be reasonably explained.

This last example we have shown is a remarkable and very recent one of positive interaction between cloud physics and radar meteorology. CDR radar has shown capabilities in distinguishing large, non-spherical, non-Rayleigh scatterers, and small Rayleigh scatterers, be they of water or ice, but more laboratory or theoretical cloud physics investigations are essential in fully exploiting the microphysical information provided by the CDR radar.

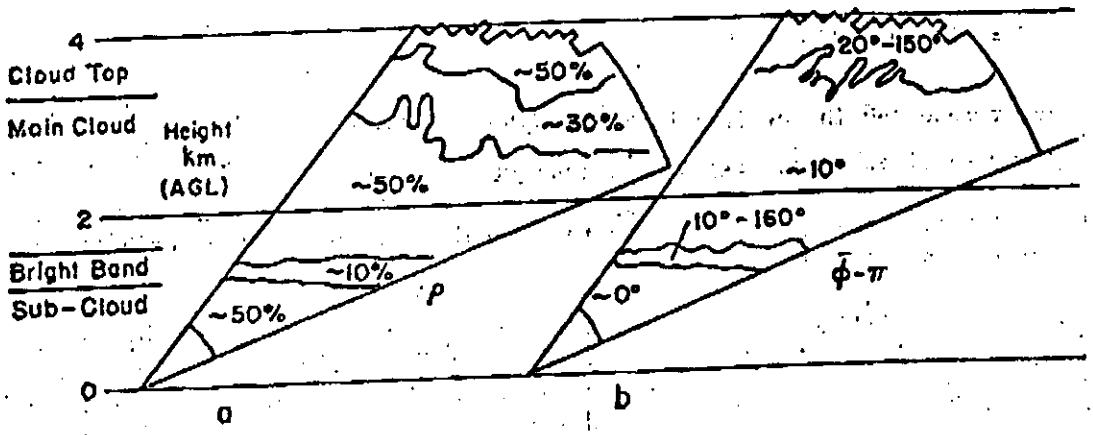

Figure 10 - Magnitude (a) and phase (b) of the cross correlation between main and cross polarization channels for 15 June 1981, 1331:04-1332:35 LT.

REFERENCES

Freire, E., and List, R., 1979: Collision enhancement for droplets pairs with electrically reduced approach speed, J.Atm.Sc.36

Kropfli, R.A., Moninger, W.R. and Pasqualucci, F., 1982: Cloud particle identification near the melting layer with dual polarization K band doppler radar

Levi, L. and Prodi, F., 1978: Crystal size in accreted ice, J.Atm.Sc.35

Low, T.B. and List, R., 1982: Collision, coalescence and breakup of raindrops. Part I: Experimentally established coalescence efficiencies and fragment size distributions in breakup. J.Atm.Sc.39, 1591-1618

Mininger, W.R., Kropfli, R.A. and Pasqualucci, F., 1982: Hydrometeor orientations and alignment as measured by dual polarization doppler radar during CCOPE

Prodi, F. and Levi, L., 1980: Aging of accreted ice, J.Atm.Sc.37

Prodi, F., Caporaloni, M., Santachiara, G. and Tampieri, F., 1981: Inertial capture of droplets by obstacles in the form of disks and stellar crystals. Q.J. Roy. Met. Soc., 107, 699-710

Rasmussen, R.M., Levizzani, V. and Pruppacher, H., 1982: A theoretical and wind tunnel study of the melting behaviour of small and large spherical ice particles